MATERIAL NONLINEAR ANALYSIS OF STEEL FIBRE REINFORCED CONCRETE BEAMS FAILING IN SHEAR

Joaquim Barros[1], Ravindra Gettu[2], Bryan Barragán[2]
[1] University of Minho, [2] Universitat Politecnica de Catalunya, Spain

Abstract
Experimental research has pointed out that fibre reinforcement gives valuable contribution for the shear strength of concrete beams. To obtain data to check the validity of the formulation proposed by RILEM TC 162-TDF for the evaluation of the fibres contribution for the concrete shear strength, sets of concrete beams were tested experimentally. To simulate the behaviour of this kind of structures, a computational code was developed, based on the finite element techniques. An accurate simulation of the behaviour of structures failing in a brittle mode, such is the case of the beams failing in shear, is a true challenge in the computational mechanics domain. To reproduce with enough accuracy the fracturing process of this type of elements, a multifixed crack model is implemented. The ability of the post-cracking stress-strain diagram proposed by RILEM TC 162-TDF to simulate the crack propagation is checked. A strain softening trilinear diagram is also derived from inverse analysis using the force-deflection relationship obtained in RILEM three-point notched beam tests. Its capability to model the fracture mode I is also assessed. The numerical strategy developed is described in the present work and the appropriateness of the model is evaluated simulating some beams tested experimentally.

1. Introduction

One of the most promising uses of steel fibres on the concrete technology is in the increase of concrete shear strength. In current applications, costs requirements advice to avoid total replacement of steel stirrups by steel fibres. Partial replacement is current practice in parts of the structures with high percentage of stirrups where, due to concrete pouring difficulties, the desired concrete quality might be not assured. Technical and economical benefits, however, were pointed out in shallow beams of high strength concrete, where stirrups were totally replaced by steel fibres [1].
To assess the efficacy of the fibre reinforcement for the concrete shear strength, series of beams of rectangular and T cross-sections reinforced with 40 kg/m^3 of hooked ends steel fibres were tested [2]. Flexural bending tests with notched steel fibre reinforced concrete (SFRC) specimens were also carried out according to the recommendations of RILEM TC 162-TDF [3] for evaluating the equivalent (f_{eq}) and the residual (f_R) flexural tensile strength parameters of the SFRC applied in the beams [2]. The values of these parameters and the ultimate load of the SFRC beams were used to check the validity of the formulation proposed by RILEM TC 162-TDF [4] for the simulation of the contribution of the fibre addition to the concrete shear strength [2].

Fax: +351 253510217
E-mail: .barros@civil.uminho.pt

To predict the deformability, the load carrying capacity and the crack pattern of elements reinforced with conventional and steel fibres, a numerical model based on the finite element techniques and including constitutive laws for modelling the nonlinear behaviour of the intervening materials was developed. Special care was taken in the simulation of the post-cracking behaviour, since it is the main property benefited by fibre reinforcement. Due to lack of space, this work only leads with the beams of series S1 represented in Fig. 1 [2]. The evaluated concrete properties are indicated in Table 1.

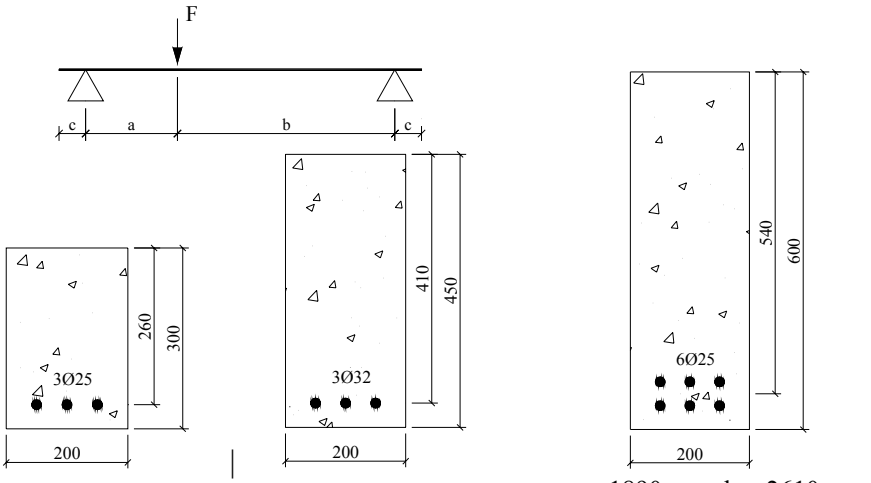

a = 910 mm; b = 1290 mm | a = 1370 mm; b = 1930 mm | a = 1890 mm; b = 2610 mm

(a) (b) (c)

Fig. 1 - SFRC-20x30_S1 (a); SFRC-20x45_S1 (b) and SFRC-20x60_S1 (c) of beams of series S1 [2].

Table 1 - Concrete properties of the beams of series S1.

Concrete	f_c [MPa]	$f_{eq,2}$ [MPa]	$f_{eq,3}$ [MPa]	$f_{R,1}$ [MPa]	$f_{R,4}$ [MPa]
Plain concrete	32.1 (±2%)	-	-	-	-
SFRC-1	37.7 (±2%)	5.85 (±15%)	6.39 (±12%)	5.96 (±10%)	5.99 (±10%)

2. Constitutive model

The concrete cracking is simulated under the framework of the multifixed smeared crack concepts [5]. According to the present model, the total strain increment of the cracked concrete, $\Delta\underline{\varepsilon}$, is the addition of the strain increment in the fracture zone, $\Delta\underline{\varepsilon}^{cr}$, with the strain increment of the concrete between cracks, $\Delta\underline{\varepsilon}_{ep}^{co}$:

$$\Delta\underline{\varepsilon} = \Delta\underline{\varepsilon}_{ep}^{co} + \Delta\underline{\varepsilon}^{cr} \quad (1)$$

Joaquim Barros, Material nonlinear analysis of steel fibre, 2/10
Fax: +351 253510217
E-mail: .barros@civil.uminho.pt

The concrete between cracks can be in elastic (*e*) or in elasto-plastic (*ep*) behaviour. In the last case, associated elasto-plastic theory is used to obtain plastic deformation and to assure the material does not violate its yield surface [7]. The concrete is governed by the following constitutive equation:

$$\Delta\underline{\sigma}=\underline{D}^{co}\Delta\underline{\varepsilon}^{co} \tag{2}$$

where, in the case of uncracked linear-elastic material, $\underline{D}^{co}$ becomes with the designation of $\underline{D}_e^{co}$, with the following format:

$$\underline{D}^{co} \rightarrow \underline{D}_e^{co} = \frac{E_c}{1-\upsilon_c^2}\begin{bmatrix} 1 & \upsilon_c & 0 \\ \upsilon_c & 1 & 0 \\ 0 & 0 & \dfrac{1-\upsilon_c}{2} \end{bmatrix} \tag{3}$$

where υ_c and E_c are the Poisson coefficient and the Young's modulus of the uncracked concrete. When cracked, but with the concrete between cracks in linear-elastic behaviour, $\underline{D}^{co}$ has the following configuration [6]:

$$\underline{D}^{co} \rightarrow \underline{D}_{ecr}^{co} = \left\{\underline{D}_e^{co} - \underline{D}_e^{co}\,\underline{T}^{crT}\left[\underline{D}^{cr} + \underline{T}^{cr}\,\underline{D}_e^{co}\,\underline{T}^{crT}\right]^{-1}\underline{T}^{cr}\,\underline{D}_e^{co}\right\} \tag{4}$$

where $\underline{T}^{cr}$ is a matrix defining the orientation of the cracks formed at a sampling point. If *m* cracks occurs at a sampling point:

$$\underline{T}^{cr} = \left[\underline{T}_1^{cr} \;,\; \underline{T}_i^{cr} \;,\; \underline{T}_m^{cr}\right]^T \tag{5}$$

where the crack orientation of a generic *ith* crack is defined by the matrix $\underline{T}_i^{cr}$:

$$\underline{T}_i^{cr} = \begin{bmatrix} \cos^2\theta_i & \sin^2\theta_i & 2\sin\theta_i\cos\theta_i \\ -\sin\theta_i\cos\theta_i & \sin\theta_i\cos\theta_i & \cos^2\theta_i-\sin^2\theta_i \end{bmatrix} \tag{6}$$

with θ_i being the angle between x_1 and the normal to the *ith* crack plane (see Fig. 2). In (4) $\underline{D}^{cr}$ is a matrix including the constitutive law of the cracks:

$$\underline{D}^{cr} = \begin{bmatrix} \underline{D}_1^{cr} & \ldots & \underline{0} & \ldots & \underline{0} \\ \ldots & \ldots & \ldots & \ldots & \ldots \\ \underline{0} & \ldots & \underline{D}_i^{cr} & \ldots & \underline{0} \\ \ldots & \ldots & \ldots & \ldots & \ldots \\ \underline{0} & \ldots & \underline{0} & \ldots & \underline{D}_m^{cr} \end{bmatrix} \tag{7}$$

where $\underline{D}_i^{cr}$ is the *ith* crack constitutive law:

$$\underline{D}_i^{cr} = \begin{bmatrix} D_{I,i}^{cr} & 0 \\ 0 & D_{II,i}^{cr} \end{bmatrix} \tag{8}$$

Joaquim Barros, Material nonlinear analysis of steel fibre, 3/10
Fax: +351 253510217
E-mail: .barros@civil.uminho.pt

with D_I^{cr} and D_{II}^{cr} being the crack fracture mode I and mode II stiffness modulus, respectively. The crack system of a sampling point is governed by the following relationship:

$$\Delta\underline{\sigma}^{cr} = \underline{D}^{cr}\Delta\underline{\varepsilon}^{cr} \tag{9}$$

where $\Delta\underline{\sigma}^{cr}$ is the vector of the incremental crack stress components (Fig. 2):

$$\Delta\underline{\sigma}^{cr} = \left[\Delta\sigma_{n,1}^{cr} \quad \Delta\tau_{nt,1}^{cr} \quad \ldots \quad \Delta\sigma_{n,i}^{cr} \quad \Delta\tau_{nt,i}^{cr} \quad \ldots \quad \Delta\sigma_{n,m}^{cr} \quad \Delta\tau_{nt,m}^{cr}\right]^T \tag{10}$$

and $\Delta\underline{\varepsilon}^{cr}$ is the vector of the incremental crack strain components:

$$\Delta\underline{\varepsilon}^{cr} = \left[\Delta\varepsilon_{n,1}^{cr} \quad \Delta\gamma_{nt,1}^{cr} \quad \ldots \quad \Delta\varepsilon_{n,i}^{cr} \quad \Delta\gamma_{nt,i}^{cr} \quad \ldots \quad \Delta\varepsilon_{n,m}^{cr} \quad \Delta\gamma_{nt,m}^{cr}\right]^T \tag{11}$$

The D_I^{cr} of (8) is characterised by the fracture parameters (see Fig. 3), namely, the tensile strength, $\sigma_1^{cr} = f_{ct}$, the fracture energy, G_f, the shape of the softening law and the crack bandwidth, l_b. Fibre reinforcement mechanisms are reflected, mainly, on the energy dissipated in the mode I fracturing process and on the shape of the softening branch. For fibre contents used in current concrete applications, the remaining concrete properties are only marginally affected by fibre addition [5]. The crack mode I stiffness is simulated by the trilinear diagram represented in Fig. 3.

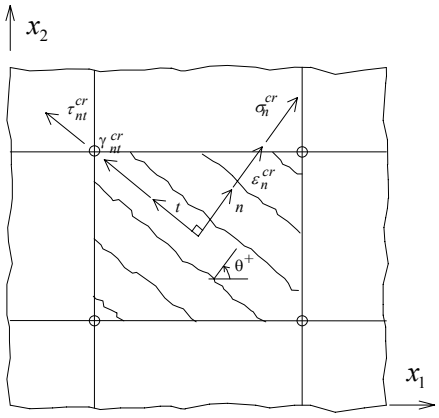

Fig. 2 - Crack stress and crack strain components

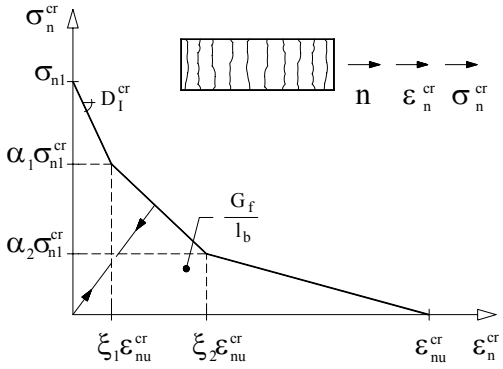

Fig. 3 - Trilinear softening diagram

The fracture mode II modulus, D_{II}^{cr}, is obtained from the expression [5, 6]:

$$D_{II}^{cr} = \frac{\beta}{1-\beta}G_c \tag{12}$$

where G_c is the concrete shear modulus and,

Joaquim Barros, Material nonlinear analysis of steel fibre, 4/10
Fax: +351 253510217
E-mail: .barros@civil.uminho.pt

$$\beta = \left[1 - \frac{\varepsilon_n^{cr}}{\varepsilon_{nu}^{cr}}\right]^p \quad (p=1,\ 2 \text{ or } 3) \tag{13}$$

is the shear retention factor, with ε_{nu}^{cr} being the ultimate normal crack strain (Fig. 3).

If concrete is uncracked and plastic deformations occurred due to compression, $\underline{D}^{co}$ of (2) is replaced by the consistent tangent operator, $\underline{D}_{ep}^{co}$ (associated flow rule and isotropic hardening approaches were assumed [6, 9]):

$$\underline{D}^{co} \rightarrow \underline{D}_{ep}^{co} = \underline{H} - \frac{\underline{H}\,\dfrac{\partial f}{\partial \underline{\sigma}}\left(\dfrac{\partial f}{\partial \underline{\sigma}}\right)^T \underline{H}}{h + \left(\dfrac{\partial f}{\partial \underline{\sigma}}\right)^T \underline{H}\,\dfrac{\partial f}{\partial \underline{\sigma}}} \tag{14}$$

where

$$\underline{H} = \left[\left[\underline{D}_e^{co}\right]^{-1} + \Delta\lambda \frac{\partial^2 f}{\partial \underline{\sigma}^2}\right]^{-1} \tag{15}$$

is a matrix that includes effects of plastic flow, $\Delta\lambda$ is the (finite) amount of plastic flow within a loading step, and

$$f\left(\underline{\sigma}, \kappa\right) = \left(\underline{\sigma}^T \underline{P}\,\underline{\sigma}\right)^{1/2} + \underline{q}^T \underline{\sigma} - \bar{\sigma}\left(\kappa\right) = 0 \tag{16}$$

is the yield function, where

$$\underline{P} = \begin{bmatrix} a & b & 0 \\ b & a & 0 \\ 0 & 0 & c \end{bmatrix},\ \underline{q} = d\underline{q}_1 = d\begin{bmatrix} 1 & 1 & 0 \end{bmatrix}^T \tag{17}$$

are the projection matrix and the projection vector [6], respectively, with

$$a = \left(\frac{a_0}{2}\right)^2 + b_0,\quad b = \left(\frac{a_0}{2}\right)^2 - \frac{b_0}{2},\quad c = 3b_0,\quad d = \frac{a_0}{2},\quad a_0 = 0.355,\quad b_0 = 1.355 \tag{18}$$

In (13) h is the hardening modulus, that can be obtained derivating the yield function, f, in relation to the hardening parameter, k:

$$h = \frac{\partial f}{\partial \kappa} = \frac{d\bar{\sigma}\left(\kappa\right)}{d\kappa} \tag{19}$$

In (16) $\bar{\sigma}\left(\kappa\right)$ is the effective compressive stress and k is the hardening parameter. The fibre influence on the concrete uniaxial behaviour is only significant on the post-peak softening phase [5]. Therefore, the $\bar{\sigma}\left(\kappa\right)$ was defined from the stress-strain relationship proposed by CEB-FIP 1993 [7] for the plain concrete, where k is transformed in an effective plastic strain using a work hardening approach [6].

For the cracked concrete with concrete between cracks in elasto-plastic behaviour, $\underline{D}^{co}$ of (2) is replaced by:

$$\underline{D}^{co} \rightarrow \underline{D}_{epcr}^{co} = \left\{\underline{D}_{ep}^{co} - \underline{D}_{ep}^{co}\,\underline{T}^{crT}\left[\underline{D}^{cr} + \underline{T}^{cr}\,\underline{D}_{ep}^{co}\,\underline{T}^{crT}\right]^{-1}\underline{T}^{cr}\,\underline{D}_{ep}^{co}\right\} \tag{20}$$

Joaquim Barros, Material nonlinear analysis of steel fibre, 5/10
Fax: +351 253510217
E-mail: .barros@civil.uminho.pt

In the simulations of the present work, a maximum number of three cracks per sampling point can be formed, according to the following criteria: the maximum principal stress attains the tensile strength and the angle between the new crack and the previous cracks is greater than a threshold angle. In the simulations carried out a threshold angle of 30 degrees was considered. A sub-incrementation procedure on the $\Delta\underline{\varepsilon}$ is performed to accomplish this criteria, and to account for the crack status changes resulting from crack initiation, closing and reopening. In a sampling point, when a new crack is formed, the fracture energy attributed to this crack is function of the material fracture energy, the energy dissipated for previous cracks and the relative orientation amongst the cracks [6].

3. Assessing the fracture parameters from inverse analysis

To assess the concrete fracture parameters, an inverse analysis was performed, evaluating the values of the σ_{ni}^{cr} and ε_{ni}^{cr} of the $\sigma_n^{cr}-\varepsilon_n^{cr}$ diagram (Fig. 3) that fit the experimental $F-\delta$ curves with the minimum error of the parameter

$$err = \left| A_{F-\delta}^{\exp} - A_{F-\delta}^{num} \right| \Big/ A_{F-\delta}^{\exp}, \tag{21}$$

where $A_{F-\delta}^{\exp}$ and $A_{F-\delta}^{num}$ are the areas below the experimental and the numerical $F-\delta$ curves, respectively. The test set up used for this purpose was the same recommended by RILEM TC 162 TDF for the SFRC [3]. In the numerical simulation, the crack development was restricted to the finite elements above the notch. The specimen was discretized in eight node Serendipity plane stress elements. To avoid a spurious interference of the fracture mode II in the specimen deformational response, two sampling points per element placed at the specimen's symmetry axis composed the integration scheme of these elements. In the remaining elements, a 2×2 Gauss-Legendre integration rule was applied. The adequacy of the numerical strategy adopted is shown in Fig. 4, revealing that the proposed trilinear $\sigma_n^{cr}-\varepsilon_n^{cr}$ diagram is capable of predicting, with enough accuracy, the post-cracking behaviour of plain concrete (PC) and SFRC specimens. Table 2 includes the data defining the $\sigma_n^{cr}-\varepsilon_n^{cr}$ diagram, where the fracture energy was evaluated assuming the crack-band width as being equal to the notch width (5 mm). These data is the average of three tests.

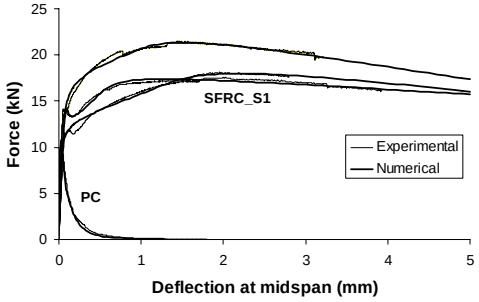

Fig. 4 – Experimental vs. numerical curves of PC and SFRC specimens

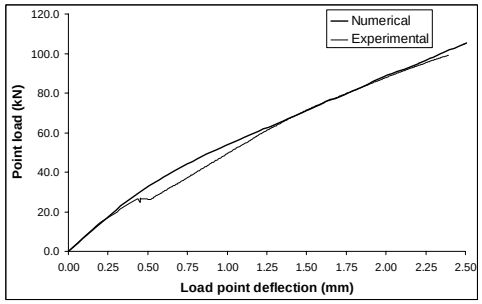

Fig. 5 - Experimental vs. numerical curves of 20x30 PC beam

Fax: +351 253510217
E-mail: .barros@civil.uminho.pt

Table 2 - Data for defining the trilinear $\sigma_n^{cr} - \varepsilon_n^{cr}$ diagram, obtained from inverse analysis

	$\sigma_{n1}^{cr} = f_{ct}$ [MPa]	$\varepsilon_{n2}^{cr} / \varepsilon_{nu}^{cr}$	$\sigma_{n2}^{cr} / \sigma_{n1}^{cr}$	$\varepsilon_{n3}^{cr} / \varepsilon_{nu}^{cr}$	$\sigma_{n3}^{cr} / \sigma_{n1}^{cr}$	G_f [N.mm/mm^2]
PC	2.600	0.0498	0.183	0.2670	0.010	0.087
SFRC	2.733	0.0096	0.727	0.0963	0.943	8.733

Previous experimental and numerical research [5] has shown that, for the type and amount of fibres used in the SFRC beams of the present work, the fracture energy would be much lower than the value obtained from inverse analysis. One possible justification resides on the fact that in the inverse analysis the crack propagation was restricted to the surface above the notch while, due to the effect of the fibre reinforcement mechanisms, cracks aside of this assumed surface are formed, resulting a fracture surface that should be much larger than the assumed one in the numerical simulation.

4. Applicability of the inverse analysis

The applicability of the inverse analysis for defining a valid $\sigma_n^{cr} - \varepsilon_n^{cr}$ diagram for the numerical simulation of beams failing in shear will be assessed analysing a PC and a SFRC beams of series S1 (SFRC-20x30_S1). The beam size effect was taken into account, following the recommendations of RILEM TC 162-TDF [4]. The data used in the numerical simulation is included in Table 3 (simulation A). Fig. 5 shows that the model can reproduces with enough accuracy the deformational behaviour of beams without any shear reinforcement (failing in shear). Since in the PC notched specimen RILEM test, the force-deflection relationship was registered up to full fracture energy dissipation, the fracture parameters obtained by inverse analysis can be directly used on the definition of the mode I crack constitutive law.

Using the fracture parameters indicated in Table 2 for SFRC, the test of the 20x30 SFRC beam of series 1 (Fig. 1) was simulated. A flexural failure mode was predicted by the numerical model, while this beam was experimentally failed in shear. Moreover, the numerical model has predicted a maximum load larger than the experimental one. This shows that the fracture parameters obtained by inverse analysis with the F-δ relationships registered in RILEM flexural tests with SFRC specimens cannot be directly used to define the $\sigma_n^{cr} - \varepsilon_n^{cr}$ diagram for the numerical simulation of beams failing in shear.

5. Applicability of the RILEM post-cracking stress-strain diagram

Fig. 6 represents the σ-ε diagram proposed by RILEM TC 162-TDF [4] to model the uniaxial behaviour of SFRC. The points defining this diagram are determined from the following relations:

$\sigma_1 = 0.7 f_{ctm,fl}$ *(1600-d)* with *1600-d* < 1.0; $E_c = 9500 (f_{cm})^{1/3}$; $\varepsilon_1 = \sigma_1 / E_c$; (22)

$\sigma_2 = 0.45 f_{R,1} \kappa_h$; $\varepsilon_2 = \varepsilon_1 + 0.1‰$; $\sigma_3 = 0.37 f_{R,4} \kappa_h$; $\varepsilon_3 = 25‰$

Joaquim Barros, Material nonlinear analysis of steel fibre, 7/10
Fax: +351 253510217
E-mail: .barros@civil.uminho.pt

where $f_{ctm,fl}$ and E_c are the SFRC average flexural tensile strength and Young's modulus, in MPa, respectively, d is the effective beam depth, in mm, and κ_h is the size effect parameter. The ability of this diagram to model the post-cracking behaviour of the SFRC will be assessed converting this relationship into a $\sigma_n^{cr} - \varepsilon_n^{cr}$ diagram and, as a title of example, simulating the SFRC-20x30_S1 beam (Fig. 1). To obtain the fracture energy from the RILEM post-cracking stress-strain relationship it was assumed for the fracture process zone a value equal to three times the fibre length (180 mm). The data used in this simulation is included in Table 3 (simulation B). As Fig. 7 shows, using the RILEM approach a flexural failure mode was predicted numerically, while the beam has experimentally failed in shear. The maximum load was larger than the value registered experimentally.

Fig. 6 - σ-ε diagram for SFRC, according to RILEM TC 162 TDF

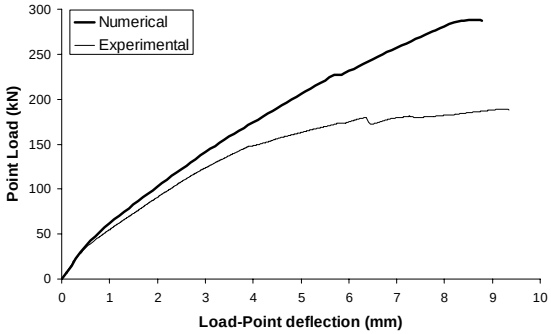

Fig. 7 - Experimental vs. numerical curves

6. Simulation of the SFRC beams of series S1

Table 3 includes the data (simulation C) used on the numerical simulation of the cross-sectional rectangular beams composing series S1 (see Fig. 1).

Table 3 - Data used in the numerical simulation

Concrete Common data: 8 node FE, 3x3 Gauss points; l_b=sqrt (area of finite element); υ_c=0.2		
Simulations		
A	B	C
	Common data: E_c=31854 MPa; f_{cm}=32.1 MPa; p=3 [expression (13)]	
E_c=29336 MPa f_{cm}=32.1 MPa fracture parameters: in Table 2 p=1 [expression (13)]	f_{ct}=3.36 MPa ξ_1=0.00385; α_1=0.62 ξ_2=0.962; α_2=0.51 G_f=8.605 N/mm	f_{ct}=2.5 MPa ξ_1=0.003; α_1=0.4 ξ_2=0.01; α_2=[0.05-0.2] G_f=[1.0-1.3] N/mm
Steel: 2 node embedded FE, 2 Gauss points; E_s=200000 MPa; f_{sy}=f_{su}=400 MPa		

Joaquim Barros, Material nonlinear analysis of steel fibre, 8/10
Fax: +351 253510217
E-mail: .barros@civil.uminho.pt

The numerical and the experimental curves of the Load-point deflection-Point load relation are represented in Fig. 8. The crack pattern at failure of the SFRC_20x60_S1 beam is shown in Fig. 9. The numerical simulations were interrupted when convergence was not possible to assure. Not only the maximum load was accurately predicted, as well as, the shear failure mode of the experimentally tested beams. The model was not, however, capable of simulating the decrease of stiffness occurred experimentally near the ultimate load. The high level of deflection at failure observed experimentally is a consequence of the stress transfer capability between crack surfaces that is assured by fibres crossing these cracks. More numerical research is being done to enhance this model deficiency.

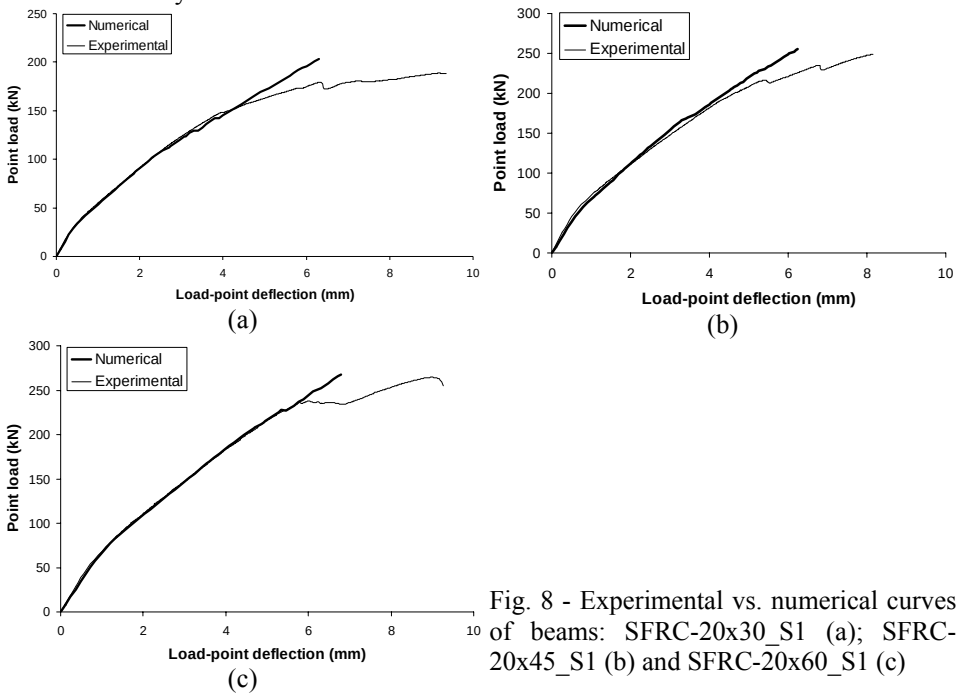

Fig. 8 - Experimental vs. numerical curves of beams: SFRC-20x30_S1 (a); SFRC-20x45_S1 (b) and SFRC-20x60_S1 (c)

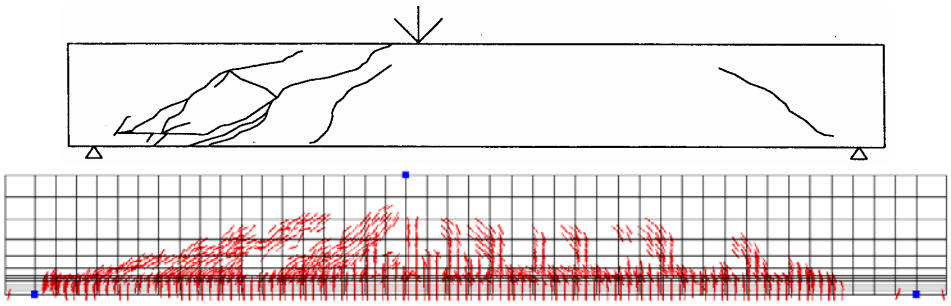

Fig. 9 – Crack pattern of SFRC-20x60_S1 (only cracks in opening process are depicted)

Joaquim Barros, Material nonlinear analysis of steel fibre, 9/10
Fax: +351 253510217
E-mail: .barros@civil.uminho.pt

7. Conclusions

To verify if post-cracking stress-strain relationship, $\sigma_n^{cr} - \varepsilon_n^{cr}$, can be defined by inverse analysis with the model developed, the concrete fracture parameters were obtained carrying out an inverse analysis with the force-deflection relationships, F-δ, obtained in three point notched beam specimens. Using these fracture parameters, the behaviour of plain (PC) and steel fibre reinforced concrete (SFRC) beams failing in shear was simulated. With the fracture parameters obtained according to this strategy, the behaviour of PC beams was accurately simulated. Since the F-δ relationship was obtained up to full energy dissipation of the PC specimens, the fracture parameters are representative of the PC post-cracking behaviour. It is only necessary to consider a size effect factor, to take into account the size of the structure in analysis. In case of SFRC specimens, however, the test is interrupted at about 5 mm, when the energy dissipated is only a fraction of the total energy consumed in the fracturing process. Therefore, the fracture parameters cannot be directly used on the definition of the $\sigma_n^{cr} - \varepsilon_n^{cr}$. To simulate the behaviour of experimentally tested SFRC beams, a trilinear $\sigma_n^{cr} - \varepsilon_n^{cr}$ diagram was defined. The developed model was able of estimating the ultimate load, the most relevant aspects of crack pattern and the deformability up to near the maximum load.

Acknowledgments

The first author wishes to acknowledge the grant SFRH/BSAB/291/2002-POCTI, provided by FCT and FSE.

References

1. Casanova, P., 'Bétons renforcés de fibres métalliques du matériau à la structure', PhD Thesis, LCPC, Paris, France, (996) 203 pgs.
2. Barragán, B.E., 'Failure and tougness of steel fiber reinforced concrete under tension and shear', PhD Thesis, UPC, Barcelona, March (2002).
3. RILEM TC 162-TDF, 'Test and design methods for steel fibre reinforced concrete - Final Recommendation, Materials and Structures', Vol.35, November 2002, pp. 579-582.
4. RILEM TC 162-TDF, 'Test and design methods for steel fibre reinforced concrete - σ - ε design method - Final Recommendation', Materials and Structures, Vol.36, October (2003), pp. 560-567.
5. Barros, J.A.O., 'Behaviour of fibre reinforced concrete - experimental and numerical analysis', PhD Thesis, Civil Eng. Dept., FEUP, Portugal, (1995) (in Portuguese).
6. Sena-Cruz, J.M.; Barros, J.A.O., Azevedo, A.F.M., "Elasto-plastic smeared crack model for concrete", Report 04-DEC/E-05, Civil Eng. Dep. Univ. Minho, (2004).
7. CEB-FIP Model Code, Comite Euro-International du Beton, Bulletin d'Information nº 213/214 (1993).

Fax: +351 253510217
E-mail: .barros@civil.uminho.pt